

Using out-of-focus light to improve image acquisition time in confocal microscopy

Brynmor J. Davis^a, William C. Karl^a, Bennett B. Goldberg^{b,a}, Anna K. Swan^a and M. Selim Ünlü^a

^aDepartment of Electrical and Computer Engineering, Boston University, 8 Saint Mary's Street, Boston, MA 02215, USA;

^bDepartment of Physics, Boston University, 590 Commonwealth Avenue, Boston, MA 02215, USA

ABSTRACT

Light that would typically be discarded at a confocal microscope's detector pinhole will be collected and processed to allow a reduced spatial sampling rate and thus an improved image acquisition time. It is shown that collecting and appropriately processing the out-of-focus light will allow an axial sampling rate below that specified by the Nyquist criterion. To achieve this, a central detector pinhole and a number of out-of-focus regions are collected concurrently. This corresponds to imaging through several different channels, with differing point spread functions, in parallel. Since the spatial sampling rate is below the Nyquist frequency, aliasing occurs in the data from each of the channels. However, since the point spread functions are different, the aliasing effects are different in each channel. This allows the ensemble of aliased images to be processed into a single dealiased and deconvolved image. This potential utility of out-of-focus light is demonstrated through simulated examples for differing collection schemes and scanning rates. Results are shown for under-sampling by up to a factor of four. Collecting the out-of-focus light also improves instrument collection efficiency.

Keywords: Confocal microscopy, image acquisition time, sampling rate, aliasing, out-of-focus light, confocal pinhole, high speed microscopy, confocal collection efficiency

1. INTRODUCTION

In confocal microscopy, a small pinhole improves axial sectioning by rejecting light arriving from out-of-focus planes. Using a large pinhole to collect more emitted light improves collection efficiency, image acquisition time and/or signal-to-noise ratio (SNR) but also suffers a worsened axial resolution. The strategy proposed here is to collect both sets of data simultaneously and under-sample. Fine detail information will be present in the small-pinhole data and much of the information lost by under-sampling can be extracted from the low-axial-resolution, large-pinhole data. In order to recover a dealiased image the microscope is modeled as a multi-channel system with sampling. Image reconstruction from this type of system has been examined in the signal processing literature and is known as the "Generalized Sampling Expansion".¹ Reconstruction from noisy data² and further generalizations of this scheme³ have also been studied. A straightforward reconstruction method suitable for this application will be presented here.

Assuming a constant dwell time per point, the reduced sampling will result in an improved image acquisition time. It also improves the efficiency of the system as a higher percentage of the emitted light is being collected to make the image. An improved efficiency will allow decreased specimen damage which is particularly important in fluorescence microscopy where photobleaching can be a significant problem.

Additional hardware will need to be added to a standard confocal microscope in order to collect the out-of-focus light. An obvious solution is to focus the emitted light on to a CCD and the out-of-focus contributions can easily be read out of the appropriate pixels. With improving CCD efficiency and noise performance this method is becoming increasingly feasible. Additionally, many high-speed confocal microscopes are starting to make use

Correspondence to Brynmor Davis
E-mail: bryn@bu.edu

of CCDs as detectors so that collection may be parallelized. Examples include spinning-disk⁴ and/or microlens⁵ systems and also multifocal multiphoton microscopy.⁶ The intention of this paper is not to propose a specific implementation for the method outlined, but rather to show that the collection of out-of-focus light may provide benefits in terms of instrument efficiency, collection time or noise considerations.

2. MATHEMATICAL SYSTEM DESCRIPTION

2.1. Multi-Channel Confocal Microscopy

A reconstruction method that incorporates both deconvolution and dealiasing is proposed. In order to perform these operations, a well-defined and accurate mathematical model must be made of the imaging system.

Simultaneous collection through more than one pinhole is performed. The relationship between the object and the data collected through each pinhole is linear and shift invariant. Linear, shift-invariant systems can be modeled by spatial-domain convolution or Fourier-domain multiplication

$$d_n(x, y, z) = h_n(x, y, z) * o(x, y, z) \quad \Leftrightarrow \quad D_n(k_x, k_y, k_z) = H_n(k_x, k_y, k_z)O(k_x, k_y, k_z) \quad (1)$$

The system corresponding to each pinhole can be considered a ‘channel’. The object is represented by $o(x, y, z)$ spatially or $O(k_x, k_y, k_z)$ in the Fourier domain. Similarly, $h_n(x, y, z)$ and $H_n(k_x, k_y, k_z)$ are spatial- and Fourier-domain representations of the n^{th} system; $d_n(x, y, z)$ and $D_n(k_x, k_y, k_z)$ are spatial- and Fourier-domain representations of the data collected through the n^{th} channel. The construction of the point spread functions (PSF) $h_n(x, y, z)$ and the optical transfer functions (OTF) $H_n(k_x, k_y, k_z)$ are well understood.⁷

2.2. Modeling Aliasing

The Nyquist criterion⁸ specifies the minimum sampling rate required to represent a band-limited signal by a countable number of regularly spaced signal samples. In one dimension this condition can be written as follows.

$$R \geq 2 \frac{k^{\text{max}}}{2\pi} \quad (2)$$

Here R is the spatial sampling rate and k^{max} is the maximum angular frequency (using the angular frequency means $k^{\text{max}}/2\pi$ is in cycles per spatial unit) for which the signal’s Fourier transform is non-zero. If the sampling rate meets this criterion then the continuous signal can be recovered from the discrete samples by the appropriate interpolation. In three dimensions it is sufficient to ensure that the one-dimensional Nyquist criterion is met in each of the three dimensions. This condition can be relaxed by making use of three-dimensional structure and non-uniform and/or non-rectangular sampling,⁹ but these methods will not be considered here.

The origins of the Nyquist theorem are apparent when sampling is represented in the Fourier domain. Consider sampling the data at spatial rates R_x , R_y and R_z in the x , y and z directions respectively.

$$\bar{d}(x, y, z) = \begin{cases} d(x', y', z')\delta(x - x', y - y', z - z') & (x', y', z') \in A \\ 0 & \text{otherwise} \end{cases} \quad (3)$$

Where A is the set of sample positions.

$$A = (\dots, \frac{2}{R_x}, \frac{1}{R_x}, 0, \frac{1}{R_x}, \frac{2}{R_x}, \dots) \times (\dots, \frac{2}{R_y}, \frac{1}{R_y}, 0, \frac{1}{R_y}, \frac{2}{R_y}, \dots) \times (\dots, \frac{2}{R_z}, \frac{1}{R_z}, 0, \frac{1}{R_z}, \frac{2}{R_z}, \dots) \quad (4)$$

The function $\bar{d}(x, y, z)$ is the discrete time representation of $d(x, y, z)$ (the over-bar will be used to indicate discrete-time functions). This is a mathematically convenient way of considering the data points gathered – i.e. they represent the weightings on delta functions placed at the sample points.

In the Fourier domain the spatial sampling results in spectral replication.

$$\bar{D}(k_x, k_y, k_z) = R_x R_y R_z \sum_{p_x, p_y, p_z \in \mathbb{Z}} D(k_x - 2\pi p_x R_x, k_y - 2\pi p_y R_y, k_z - 2\pi p_z R_z) \quad (5)$$

The continuous-time data $D(k_x, k_y, k_z)$ is limited to the box B .

$$B = \{(k_x, k_y, k_z) : k_x \in [-k_x^{max}, k_x^{max}], k_y \in [-k_y^{max}, k_y^{max}], k_z \in [-k_z^{max}, k_z^{max}]\} \quad (6)$$

While the object spectrum $O(k_x, k_y, k_z)$ may be infinite in extent, the transfer functions $H_n(k_x, k_y, k_z)$ are band-limited⁷ and thus $D(k_x, k_y, k_z)$ is also band-limited as written above. If the Nyquist criterion is satisfied then the summed spectra of Eq. 5 don't overlap and the continuous signal can be recovered by applying a low-pass filter that removes all spectra except the baseband case ($p_x = p_y = p_z = 0$). The possible complications in realizing this ideal filtering/interpolation operation are well known⁸ and won't be addressed here.

Consider the box C in Fourier-space.

$$C = \{(k_x, k_y, k_z) : k_x \in [-\pi R_x, \pi R_x], k_y \in [-\pi R_y, \pi R_y], k_z \in [-\pi R_z, \pi R_z]\} \quad (7)$$

If a Fast Fourier Transform (FFT) is taken of the data collected, then the result will correspond to a regular sampling of $\bar{D}(k_x, k_y, k_z)$ in C . For that reason the following analysis will concentrate on this domain. Note that the condition $B \subset C$ is equivalent to the Nyquist criterion and conversely $C \not\subset B$ implies that aliasing may occur.

It will be assumed that R_x and R_y satisfy the Nyquist criterion while the axial dimension will be under-sampled – i.e. R_z does not satisfy the Nyquist criterion. The under-sampling factor M will be defined as follows.

$$M = \left\lceil \frac{k_z^{max}}{\pi R_z} \right\rceil \quad (8)$$

M is the maximum number of spectra that overlap at a given (k_x, k_y, k_z) . The set of p_z indicies for the overlapping spectra at that point are those that satisfy the following equation.

$$\begin{aligned} P(k_x, k_y, k_z) &= \{p_z^1, p_z^2, \dots, p_z^M\} \\ &= \{p_z : p_z \in \mathbb{Z}, k_z - 2\pi p_z R_z \in [-k_z^{max}, k_z^{max}]\} \end{aligned} \quad (9)$$

So considering Eq. 5 on the domain C and using Eq. 1.

$$\begin{aligned} \bar{D}_n(k_x, k_y, k_z) &\propto \sum_{p_z \in P(k_x, k_y, k_z)} D_n(k_x, k_y, k_z - 2\pi p_z R_z) \\ &= \sum_{p_z \in P(k_x, k_y, k_z)} H_n(k_x, k_y, k_z - 2\pi p_z R_z) O(k_x, k_y, k_z - 2\pi p_z R_z) \end{aligned} \quad (10)$$

The equation above is simply a system of linear equations at each (k_x, k_y, k_z) point. It will be convenient to write this in matrix form.

$$\bar{\mathbf{D}}(k_x, k_y, k_z) = \mathbf{H}(k_x, k_y, k_z) \mathbf{O}(k_x, k_y, k_z) \quad (11)$$

Where

$$\begin{aligned} \bar{\mathbf{D}}(k_x, k_y, k_z) &= \begin{bmatrix} \bar{D}_1(k_x, k_y, k_z) \\ \bar{D}_2(k_x, k_y, k_z) \\ \vdots \\ \bar{D}_N(k_x, k_y, k_z) \end{bmatrix}, \quad \mathbf{O}(k_x, k_y, k_z) = \begin{bmatrix} O(k_x, k_y, k_z - 2\pi p_z^1 R_z) \\ O(k_x, k_y, k_z - 2\pi p_z^2 R_z) \\ \vdots \\ O(k_x, k_y, k_z - 2\pi p_z^M R_z) \end{bmatrix} \\ \mathbf{H}(k_x, k_y, k_z) &= \begin{bmatrix} H_1(k_x, k_y, k_z - 2\pi p_z^1 R_z) & H_1(k_x, k_y, k_z - 2\pi p_z^2 R_z) & \cdots & H_1(k_x, k_y, k_z - 2\pi p_z^M R_z) \\ H_2(k_x, k_y, k_z - 2\pi p_z^1 R_z) & H_2(k_x, k_y, k_z - 2\pi p_z^2 R_z) & \cdots & H_2(k_x, k_y, k_z - 2\pi p_z^M R_z) \\ \vdots & \vdots & \ddots & \vdots \\ H_N(k_x, k_y, k_z - 2\pi p_z^1 R_z) & H_N(k_x, k_y, k_z - 2\pi p_z^2 R_z) & \cdots & H_N(k_x, k_y, k_z - 2\pi p_z^M R_z) \end{bmatrix} \end{aligned} \quad (12)$$

This completes the mathematical description of a multi-channel confocal microscope that has sub-Nyquist axial sampling.

3. FOURIER DOMAIN RECONSTRUCTION

If a signal is sampled at a rate too coarse to capture its structure accurately, the effect in the Fourier domain is described in Eq. 5 – separate points in the original spectrum alias into the same location in the sampled signal’s spectrum. In a one-channel system this mixing cannot be undone without further information about the original signal. In a multi-channel system this is not the case.

The effects of aliasing can be removed and deconvolution performed if the object spectrum $O(k_x, k_y, k_z)$ can be recovered from the set of aliased spectra collected $\bar{D}_n(k_x, k_y, k_z)$. Inverting Eq. 11 at every (k_x, k_y, k_z) point would achieve this. However inversion at every point is not possible – even in a one-channel Nyquist-rate system, high-spatial-frequency detail is either completely lost or attenuated to a level where it is not detectable in noise. In this section a method of dealiasing/deconvolution is proposed along with a method of comparing its performance to a standard one-channel, Nyquist-rate method.

In order to invert Eq. 11, an attempt will be made to invert the matrix $\mathbf{H}(k_x, k_y, k_z)$ of Eq. 12 at each (k_x, k_y, k_z) point measured within the domain C . This immediately introduces some conditions on $\mathbf{H}(k_x, k_y, k_z)$ – there must be more non-identical rows than there are columns (i.e. $N \geq M$) which implies that the maximum under-sampling factor must be no greater than the number of different pinholes used. Even if this condition is met the matrix may still be singular or have an inverse that produces unstable results in the presence of noise.¹⁰ Ideally the system will be designed so that $\mathbf{H}(k_x, k_y, k_z)$ is well conditioned over as larger area of Fourier space as possible. To achieve this the channels must be significantly different to give dissimilar rows of $\mathbf{H}(k_x, k_y, k_z)$. Spatially this means that the aliasing effects will be different in each channel and thus easily quantified and removed.

The truncated singular value decomposition (TSVD) inverse¹¹ will be used recover the components that are observable when $\mathbf{H}(k_x, k_y, k_z)$ is singular and to provide stability in the presence of noise. The general idea of this approach is that a user-defined threshold is employed to define which components of $\mathbf{O}(k_x, k_y, k_z)$ are too strongly attenuated to recover. The inverse does not attempt to recover these components so as to avoid noise induced instability. The remaining components are estimated when the TSVD inverse is applied to $\bar{\mathbf{D}}(k_x, k_y, k_z)$. The details of this approach will be omitted as they are well explained in the literature.¹¹

Let $\mathbf{G}(k_x, k_y, k_z)$ be the TSVD inverse of $\mathbf{H}(k_x, k_y, k_z)$ at the defined threshold. $\mathbf{G}(k_x, k_y, k_z)$ will be $M \times N$. An estimate of the object spectrum is calculated as follows.

$$\begin{aligned} \hat{\mathbf{O}}(k_x, k_y, k_z) &= \mathbf{G}(k_x, k_y, k_z) \bar{\mathbf{D}}(k_x, k_y, k_z) \\ &= \mathbf{G}(k_x, k_y, k_z) \mathbf{H}(k_x, k_y, k_z) \mathbf{O}(k_x, k_y, k_z) \end{aligned} \quad (13)$$

Evaluating this equation on every measured point in C will give an object spectrum estimate on the domain B . In fact, the calculated values will be at those (k_x, k_y, k_z) positions that would have been measured if the axial sampling rate had been M times larger. This means that once the entries of $\hat{\mathbf{O}}(k_x, k_y, k_z)$ are arranged correctly and an inverse FFT is taken then the result will be an estimate of the object on a grid with spatial sampling rate MR_z . This object estimate is directly comparable to that produced by a one-channel, Nyquist-rate system.

In order to perform comparisons a measure of ‘spectral purity’ will be defined. The final expression in Eq. 13 shows how the true object spectrum is related to that estimated. Let $E_{ij}(k_x, k_y, k_z)$ be the value of the element in the i^{th} row and the j^{th} column of the product $\mathbf{G}(k_x, k_y, k_z) \mathbf{H}(k_x, k_y, k_z)$. The purity measure (which has a domain of B) is defined as follows.

$$\rho(k_x, k_y, k_z - 2\pi p_z^m R_z) = \frac{|E_{mm}(k_x, k_y, k_z)|}{\sqrt{\sum_{i=1}^M |E_{mi}(k_x, k_y, k_z)|^2}} \quad (14)$$

It can be shown that if the numerator of the above equation is 0 then the denominator must also be 0, in which case $\rho(k_x, k_y, k_z) \equiv 0$. The numerator of this term is the absolute gain given to the spectral component that should be at a given location. The denominator measures how much total gain goes to the given location. The purity will range between 1 (ideal reconstruction) and 0 which indicates that no attempt is made to reconstruct that component. The intermediate values indicate that there has been some reconstruction but residual aliasing

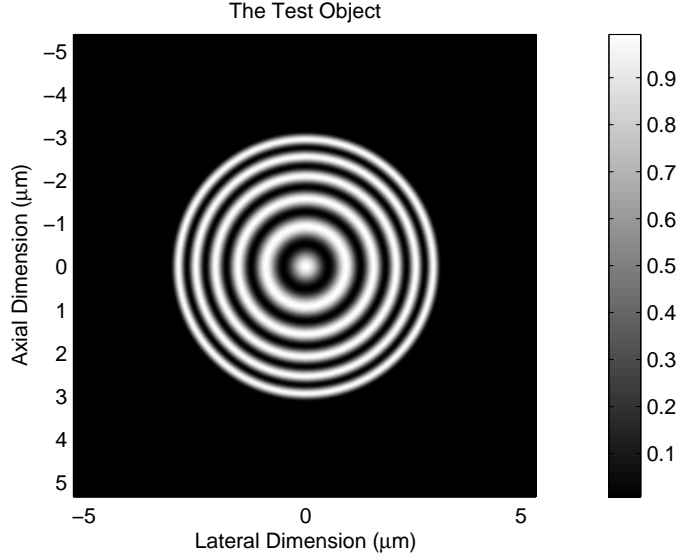


Figure 1. The test object for simulation purposes.

remains. If the product $\mathbf{G}(k_x, k_y, k_z)\mathbf{H}(k_x, k_y, k_z)$ was to be the identity (ideal imaging) then the corresponding purity measure would be all 1s.

The purity measure $\rho(k_x, k_y, k_z)$ is a tool for seeing how the reconstruction performs as a function of spatial frequency. In the case of a one-channel, Nyquist-rate system, $\mathbf{H}(k_x, k_y, k_z)$ would be a scalar (rather than a matrix) function of (k_x, k_y, k_z) . This means the reconstruction function $\mathbf{G}(k_x, k_y, k_z)$ would either be the reciprocal of $\mathbf{H}(k_x, k_y, k_z)$ (when the noise threshold is met) or 0 (when the noise threshold isn't met). A consequence of this is that the purity measure is always either 1 or 0. This is to be expected as with a Nyquist-rate system there is never going to be any contamination due to aliasing.

4. RESULTS WITH SIMULATED DATA

In this section a test object is defined along with basic instrument setups (wavelengths, sampling rates, pinhole sizes, noise levels, etc.) Reconstructions from Nyquist-rate and sub-Nyquist-rate data are compared.

4.1. The Test Object

The test object considered is a series of spheres with progressively closer spacing. The radial profile of this object is generated by a sinusoid with linearly increasing instantaneous frequency – i.e. a linear chirp. The object is approximately $6 \mu m$ in diameter. A slice of the object in the $x - z$ plane is shown in Fig. 1. Note that the object is cylindrically symmetric so this slice is sufficient to define the complete 3D object.

4.2. Instrument Parameters

A confocal fluorescence microscope will be modeled. The excitation wavelength is 488 nm and the detection wavelength is 530 nm . The excitation is circularly polarized and the emitted light is assumed to be unpolarized. These polarization states mean that the system is cylindrically symmetric and the 3D data, PSFs, OTFs, etc. can all be represented by a 2D lateral-axial slice in the figures. Four different pinholes will be used – a central circular pinhole of radius 100 nm when mapped into object space, an annulus with inner radius 100 nm and outer radius 250 nm , another annulus from 250 nm to 400 nm and finally an annulus from 400 nm to 1000 nm . The OTFs for the resulting channels are shown in Fig. 2. Qualitatively it can be seen that the OTFs are quite different which is necessary to get a well conditioned matrix $\mathbf{H}(k_x, k_y, k_z)$. As expected, it can also be seen that

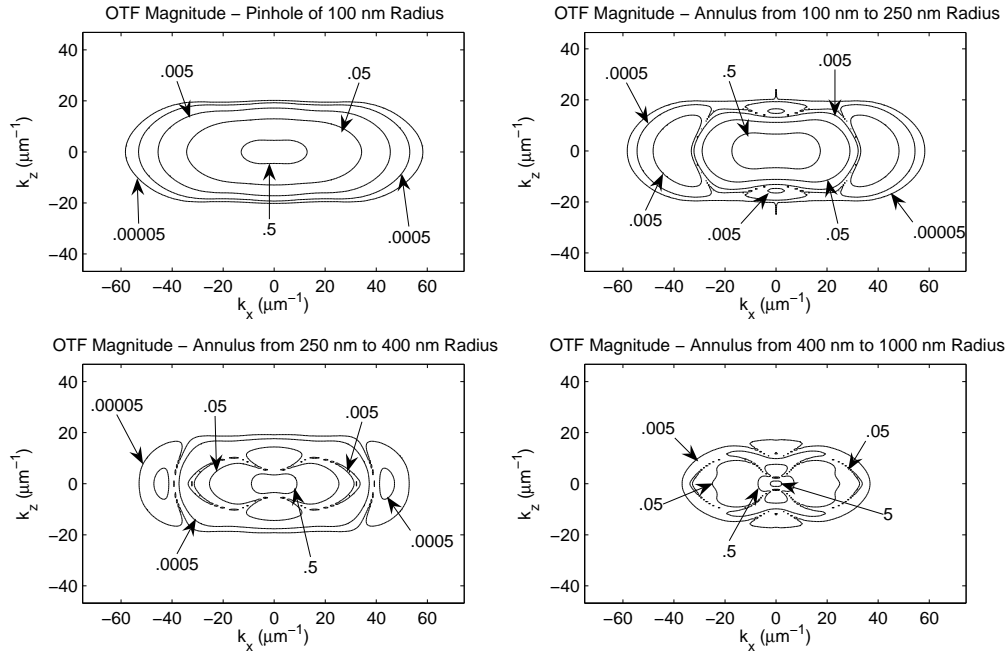


Figure 2. Contour plots of the OTFs. The plots have been normalized so that the maximum value of the central pinhole OTF is 1. Maximum values for the annuli (from the innermost to the outermost) are 3.11, 3.00 and 10.98.

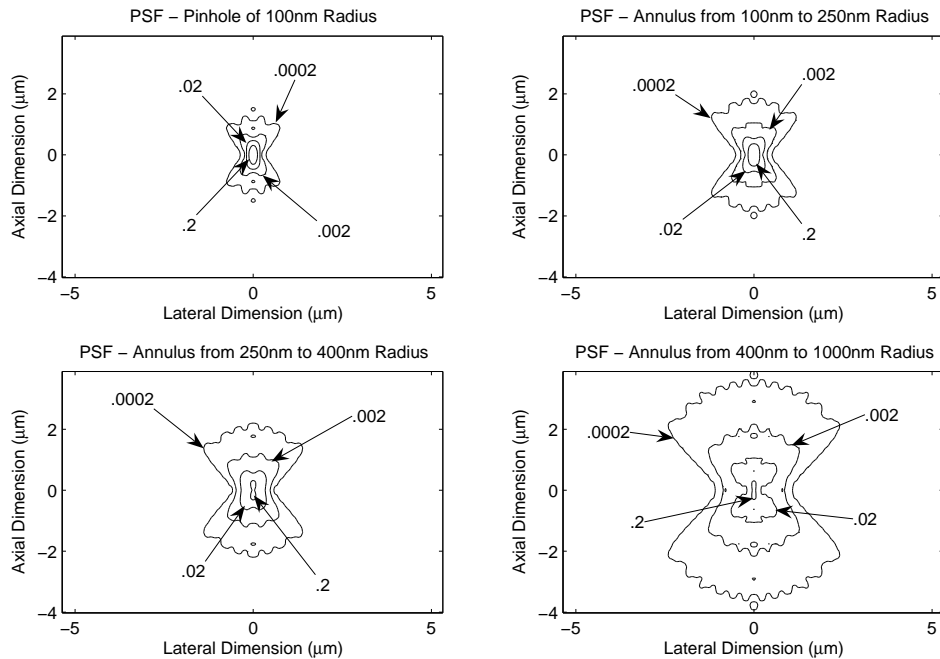


Figure 3. Contour plots of the PSFs. The plots have been normalized so that the maximum value of the central pinhole PSF is 1. Maximum values for the annuli (from the innermost to the outermost) are 1.12, 0.27 and 0.24.

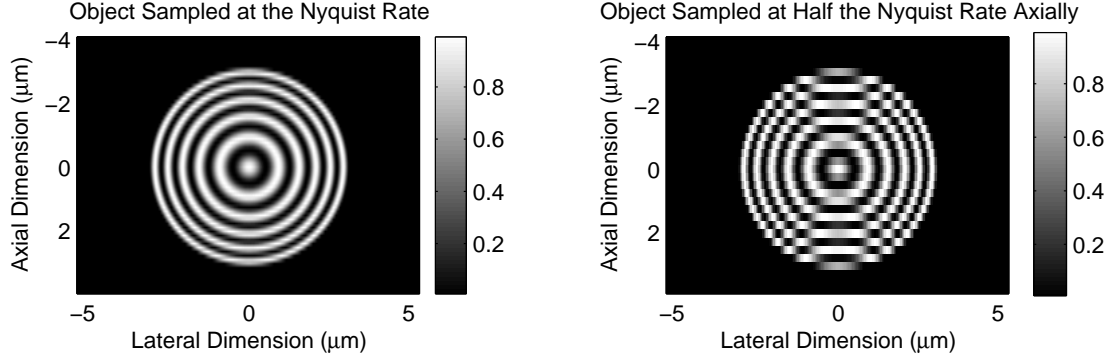


Figure 4. The test object sampled above the Nyquist rate (left) and below the Nyquist rate axially (right)

high frequencies are passed more weakly as the size of the pinhole increases. The PSFs are also shown in Fig. 3. As expected, the outer-annuli have broader PSFs and higher values off the focal plane.

The theoretical cutoffs⁷ of the OTF for an infinitely small pinhole are $67 \mu m^{-1}$ laterally and $21 \mu m^{-1}$ axially. In Fig. 2 it can be seen that the OTFs are at a very low level well before these cutoffs. Nominal lateral and axial sampling rates of $24 \mu m^{-1}$ and $8 \mu m^{-1}$ are chosen as they are slightly above the Nyquist rate as calculated with the theoretical cutoffs for an infinitely small pinhole. The object is shown sampled at this rate and at half this rate axially in Fig. 4. The effects of aliasing are clear – the areas of the object corresponding to high axial frequencies are distorted.

4.3. Noise Considerations

The reconstructions presented here are from data sampled at different rates. Sub-sampled data is synthesized by simply deleting the appropriate points from the Nyquist-rate data set. Obviously this means that corresponding points in different data sets have the same noise properties. Thus the approach taken here is to use the lesser sampling rate to achieve increased image acquisition rate. An alternative approach would be to collect longer at each point and get improved SNR for the same image acquisition time.

Two reconstructions will be presented for each system. One will be the noise-free case. This is given to show an upper-bound on what can be expected. Degradations in this image are due to residual aliasing effects and the system passing spatial-frequency components with a gain less than that defined by the user in the TSVD reconstruction. The second reconstruction shown is that produced by including Poisson noise on the data. These reconstructions give a feeling for the methods' sensitivity to noise.

4.4. Reconstructions Without Noise

A one-channel system sampled above the Nyquist rate will act as a standard comparison. The reconstruction for this system is shown in Fig. 5 along with the purity measure. As mentioned in Sect. 3, the purity measure is either 0 or 1 for the Nyquist-rate case. Those spatial frequencies that are reconstructed are marked with a 1. The threshold determines the volume of frequencies reconstructed. In this case the threshold is set to $1/20^{th}$ of the DC gain.

The next case will be a two-channel system (the central pinhole and the smallest annulus) working at half the sampling rate axially (i.e. $4 \mu m^{-1}$ rather than $8 \mu m^{-1}$). The reconstruction and spectral purity are shown in Fig. 6. The quality of this reconstruction is worse than that of the Nyquist-rate reconstruction. Aliasing degradation has not been completely removed from the high axial frequencies as can be seen in both the reconstruction and the purity measure.

Looking at Fig. 5 it can be seen that the highest axial frequency reconstructed is approximately $12 \mu m^{-1}$. The non-zero frequency components between this value and the theoretical cutoff of $21 \mu m^{-1}$ are two weakly passed to be reconstructed (at this threshold setting). An axial frequency of $12 \mu m^{-1}$ can be captured at the

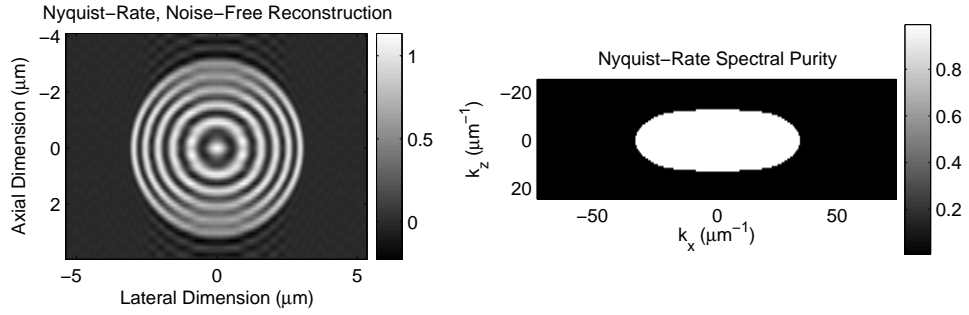


Figure 5. Noiseless Nyquist-rate reconstruction and spectral purity

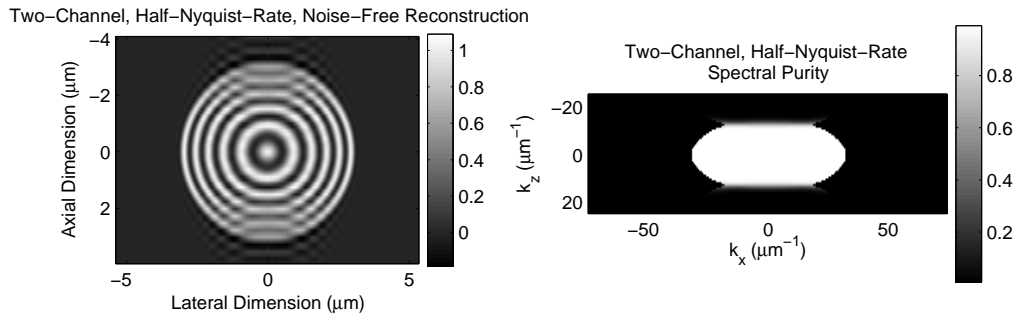


Figure 6. Noiseless two-channel, half-Nyquist-rate reconstruction and spectral purity

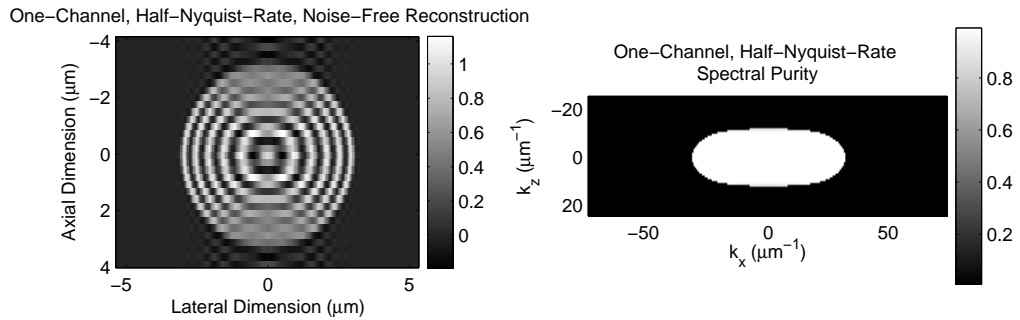


Figure 7. Noiseless one-channel, half-Nyquist-rate reconstruction and spectral purity

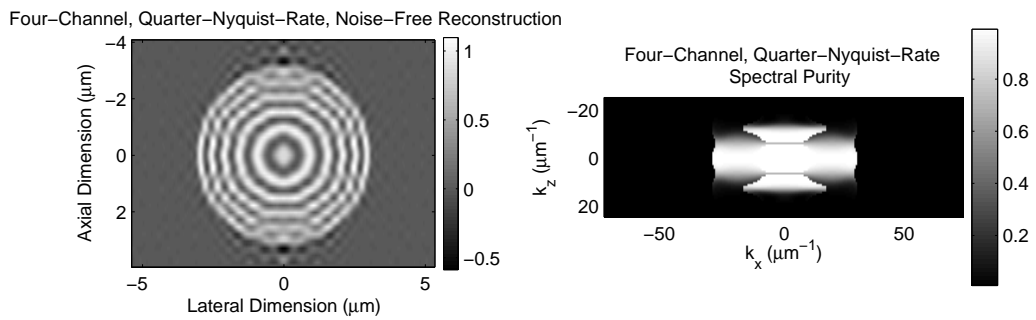


Figure 8. Noiseless four-channel, quarter-Nyquist-rate reconstruction and spectral purity

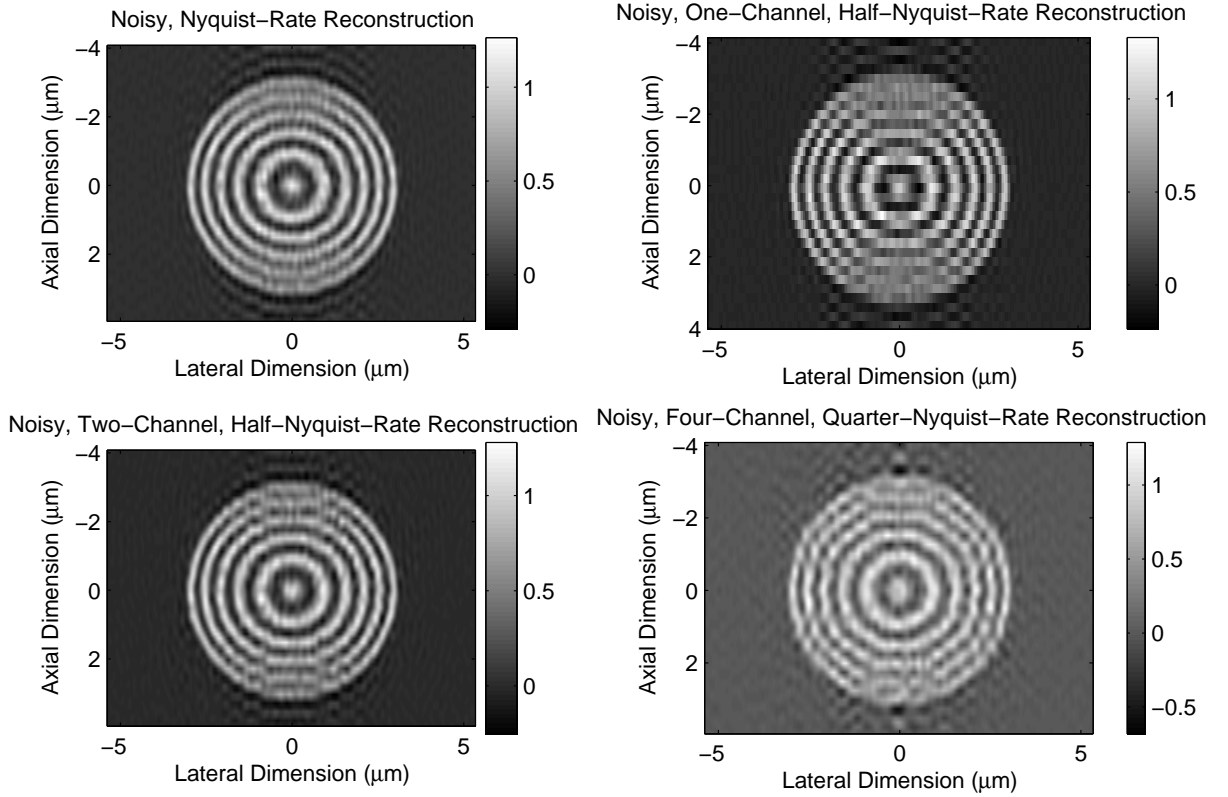


Figure 9. Noisy reconstructions for the four systems considered.

‘half-Nyquist rate’ used in the two-channel reconstruction. For comparisons sake, the reconstruction from a single channel at this rate is shown in Fig. 7. This is calculated by simply applying the same inverse filter as in the Nyquist-rate case, since the high-frequency information lost by sub-sampling is outside the pass-band of the reconstruction filter. The spectral purity is also displayed. In this case it will take on values between 0 and 1 because the weakly passed components outside the reconstruction pass-band are still present in the data and will produce aliasing.

This reconstruction is of slightly poorer quality than the two-channel case. This is to be expected as the only difference between the two systems is that an extra channel is being measured in the two-channel case. This does show that the extra channel is being processed in a useful manner.

The final noiseless case is shown in Fig. 8. Here all four apertures are used in the reconstruction and the axial sampling rate is a quarter of the nominal rate. The quality of the image has obviously suffered but the image was acquired four times faster than the Nyquist-rate reconstruction of Fig. 5.

4.5. Noisy Reconstructions

Poisson noise will now be added to the data. The maximum expected value of the central pinhole data will be set to 500 counts. In practice, the SNR of the data collected will determine what threshold is to be used in the reconstructions. In this case a count of 500, combined with the threshold used, gives reconstructions that are slightly degraded but stable in the presence of noise. A less stringent threshold would result in more noise on the reconstructions and eventually noise-induced instability, while a stricter threshold discards additional high-frequency information. The noisy reconstructions for the four cases considered in the previous section are shown in Fig. 9. It can be seen that the noise degrades the image the most in the areas of high axial spatial frequency.

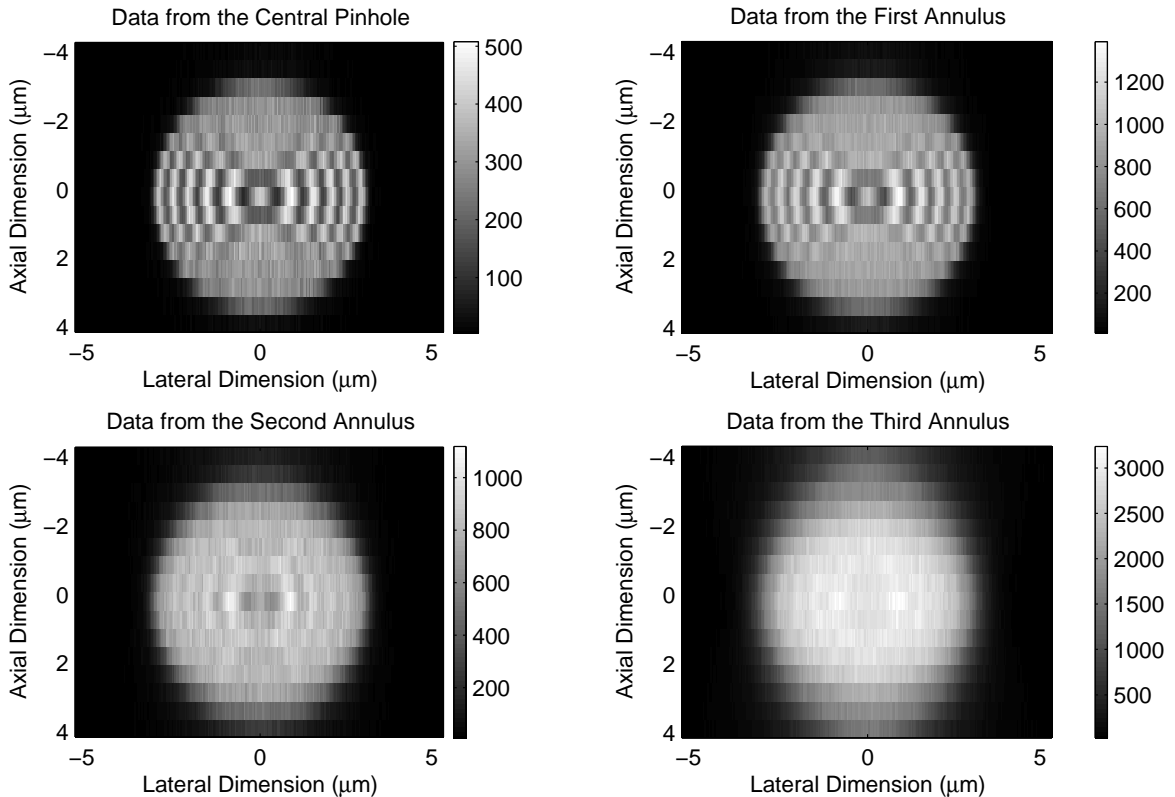


Figure 10. Raw noisy data for the four-channel, quarter-Nyquist system.

This is to be expected, as higher gains are required to recover these areas. Arguably, all of the reconstruction methods perform in a manner relatively similar to the noiseless case at this noise level.

Finally, Fig. 10 shows the noisy raw data that the four-channel, quarter-Nyquist-rate system collects. Examining this data shows that the method has indeed performed both dealiasing and deconvolution in order to get to the reconstruction of Fig. 9.

5. DISCUSSION

The results shown here have indicated that there is potential to usefully process out-of-focus light in confocal microscopy. With the increasing efficiency and reduced noise of CCDs, their use as detectors may become practical for this application. The concentration was on allowing an improved image acquisition time but of course longer could be spent collecting at each point (for the same acquisition time) and an improved SNR may result. Alternatively, out-of-focus information could be added to a Nyquist-rate system solely to improve collection efficiency.

Collecting out-of-focus light improves instrument efficiency, which is of great importance in fluorescence microscopy, particularly in low photon count, single molecule studies. However not all aliasing artifacts were completely removed, so there is now the potential to trade aliasing corruption, SNR, image acquisition time and instrument efficiency against each other. Quantifying these trade offs is the subject of future work. A physical demonstration is also planned.

The reconstruction method used here is quite straightforward. It does allow easy comparisons and conceptually simple processing. However the TSVD does have limitations. The sharp cutoff criteria has a tendency to

result in ‘ringing’ artifacts in the reconstructions. It has also produced non-physical reconstructions in that they have values below 0. These issues can be addressed by more sophisticated approaches. It is worth noting that the Fourier domain method proposed can also be cast in the spatial domain by using linear filters, summation operations and modulations (to achieve frequency shifts). Approximations to the filters may allow fast on-line processing.

The largest sampling rate reduction demonstrated is a factor of 4. That corresponds to a sampling period of 500 nm. A reduction significantly higher than this will not be possible with the system used here, as all of the PSFs have most of their energy within an axial range on the order of this size. This factor of 4 is significantly less than the orders-of-magnitude speed improvements that can be achieved by using a parallelized system such as a spinning-disk confocal microscope. However, this work demonstrates that potentially useful information is present in the out-of-focus light. Microscopes are typically parallelized laterally. This allows the potential to include the axial out-of-focus information in the parallelized systems too.

ACKNOWLEDGMENTS

This work was partially supported by the NIH under grant NIH R01 EB756-01, by the NSF under grant NSF BDI 0138425 and by the Engineering Research Centers Program of the National Science Foundation under award number EEC-9986821.

REFERENCES

1. A. Papoulis, “Generalized sampling expansion,” *IEEE Trans. Circuits Syst.* **CAS-24**, pp. 652–654, 1977.
2. N. P. Galatsanos, A. K. Katsaggelos, R. T. Chin, and A. D. Hillery, “Least squares restoration of multi-channel images,” *IEEE Trans. Sig. Proc.* **39**, pp. 2222–2236, 1991.
3. R. Venkataramani and Y. Bresler, “Sampling theorems for uniform and periodic nonuniform MIMO sampling of multiband signals,” *IEEE Trans. Sig. Proc.* **51**, pp. 3152–3136, 2003.
4. G. Q. Xiao, T. R. Corle, and G. S. Kino, “Real-time confocal scanning optical microscope,” *Appl. Phys. Lett.* **53**, pp. 716–718, 1988.
5. A. Ichihara, T. Tanaami, K. Isozaki, Y. Sugiyama, Y. Kosugi, K. Mikuriya, M. Abe, and I. Uemura, “High-speed confocal fluorescence microscopy using a Nipkow scanner with microlenses for 3D-imaging of single fluorescent molecule in real time,” *Bioimages* **4**, pp. 52–62, 1996.
6. J. Bewersdorf, R. Pick, and S. W. Hell, “Multifocal multiphoton microscopy,” *Opt. Lett.* **23**, pp. 655–657, 1998.
7. M. Gu and C. J. R. Sheppard, “Confocal fluorescent microscopy with a finite-sized circular detector,” *J. Opt. Soc. Am. A* **9**, pp. 151–153, 1992.
8. A. V. Oppenheim and R. W. Schaffer, *Discrete-Time Signal Processing*, Pearson Education, second ed., 1998.
9. K. F. Cheung and R. J. Marks II, “Imaging sampling below the Nyquist density without aliasing,” *J. Opt. Soc. Am. A* **7**, pp. 92–105.
10. W. C. Karl, “Regularization in image restoration and reconstruction,” in *Handbook of Image and Video Processing*, A. Bovik, ed., ch. 3, pp. 141–161, Academic Press, 2000.
11. P. C. Hansen, *Rank-Deficient and Discrete Ill-Posed Problems*, SIAM, 1998.